Journal of Biomedical Optics

BiomedicalOptics.SPIEDigitalLibrary.org

Assessment of tissue heating under tunable near-infrared radiation

Joel N. Bixler
Brett H. Hokr
Michael L. Denton
Gary D. Noojin
Aurora D. Shingledecker
Hope T. Beier
Robert J. Thomas
Benjamin A. Rockwell
Vladislav V. Yakovlev

SPIE.

Assessment of tissue heating under tunable near-infrared radiation

Joel N. Bixler,[a,b,†] Brett H. Hokr,[a,c,†] Michael L. Denton,[d] Gary D. Noojin,[d] Aurora D. Shingledecker,[d] Hope T. Beier,[b] Robert J. Thomas,[b] Benjamin A. Rockwell,[b] and Vladislav V. Yakovlev[a,c,*]
[a]Texas A&M University, Department of Biomedical Engineering, College Station, Texas 77843
[b]711th Human Performance Wing, Human Effectiveness Directorate, Bioeffects Division, Optical Radiation Bioeffects Branch, JBSA Fort Sam Houston, Texas 78234
[c]Texas A&M University, Department of Physics and Astronomy, College Station, Texas 77843
[d]TASC, Inc., San Antonio, Texas 78227

Abstract. The time-temperature effects of laser radiation exposure are investigated as a function of wavelength. Here, we report the thermal response of bulk tissue as a function of wavelength from 700 to 1064 nm. Additionally, Monte Carlo simulations were used to verify the thermal response measured and predict damage thresholds based on the response. [DOI: 10.1117/1.JBO.19.7.070501]

Keywords: thermography; laser-thermal tissue response.

Paper 140256LR received Apr. 23, 2014; revised manuscript received May 24, 2014; accepted for publication Jun. 11, 2014; published online Jul. 9, 2014.

Nonlinear microscopic techniques such as multiphoton fluorescent microscopy[1,2] have opened the door to noninvasive, high-resolution, deep-tissue imaging. These techniques allow for increased rejection of stray signal, as well as for the use of near-infrared (NIR) excitation wavelengths.[3,4] Three NIR optical windows have been identified, allowing for increased penetration depth for optical imaging techniques.[5] The imaging depth for such multiphoton techniques is partially limited by the amount of excitation radiation that can safely be delivered to the tissue surface, as well as the damage threshold at the focal point. Here, we examine the thermal response, measured as laser-induced temperature rise, of bulk tissue as a function of wavelength. Laser-induced heating of tissue has been shown to be linear to the incident power at a given wavelength;[6] thus the estimates for the amount of power that can be used without causing thermal damage could be extrapolated. With a lower thermal damage potential, the incident power can be increased, allowing for further increases in the maximum imaging depth of multiphoton techniques.

*Address all correspondence to: Vladislav V. Yakovlev, E-mail: yakovlev@bme.tamu.edu

†These authors contributed equally to this work.

Many multiphoton fluorescence microscopy studies utilize 800-nm excitation radiation. This is primarily due to the high-peak power and broad commercial availability of titanium-doped sapphire imaging systems, as well as the availability of commercial two-photon dyes that absorb in this range. As high-powered short-pulse optical parametric oscillators (OPOs) and optical parametric amplifiers become more common in research laboratories, additional freedom is afforded to more carefully choose the excitation wavelength. The examination of thermal damage has been limited to single wavelengths.[7,8] As thermal damage has been shown to be a major contributor to photodamage in multiphoton imaging,[7] examination of the thermal response of tissue could allow for imaging of greater depths with multiphoton techniques, especially for label-free techniques such as coherent anti-Stokes Raman scattering.[9–11]

To obtain the high level of wavelength tenability necessary in our study, a picosecond OPO (PT257; Ekspla, Vilnius, Lithuania) was used as the excitation source for thermal imaging. This source produced 5-ps pulses at a rate of 88 MHz with a maximum power of 400 mW, and a tunable range from 690 to 990 nm. Measurements were collected from a range of 700 to 950 nm in 50-nm steps, and the residual light from the internal pump laser was used for a 1064-nm data point. The laser radiation was delivered to the microscope via a 400-μm core multimode fiber. The distal tip of the fiber was imaged onto the sample surface at a 1.25× magnification, producing a 500-μm flat-top excitation spot. In order to control the laser power measured at the image plane, the laser was introduced to a polarizing cube, producing linearly polarized light which could then be attenuated by a half-wave plate. The half-wave plate was adjusted such that 82 ± 2 mW of average power (42 ± 1 W/cm^2) was measured at the image plane for all wavelengths. The thermal profile was recorded at 800 Hz using a 192×192 pixels subarray on a thermal camera (SC4000; FLIR, Wilsonville, Oregon). The thermal camera imaged the epithelial surface of the tissue sample at 3.5× magnification, resulting in a field of view of 1.6 mm with 8.6-μm resolution. A dichroic beamsplitter (BSP-DI-50-2; ISP Optics, Irvington, New York) was used to separate the IR radiation needed for thermal imaging (3 to 5 μm) from the excitation radiation. The experimental setup is depicted in Fig. 1. The sample stage was contained inside an acrylic box that was maintained at a constant 34°C, allowing the tissue sample to be held at a physiologically relevant temperature prior to laser exposure. The laser was delivered from the bottom of the box, so tissue samples were placed epithelium down on a 100-μm thick coverslip.

Porcine tissue, taken from the flank of a Yucatan mini pig, was used as an analogue for human tissue for these experiments. Tissue sections were cut using an 8 mm punch biopsy and had a thickness of greater than 10 mm, insuring sufficient volume to provide an accurate analogue to bulk tissue [see Fig. 2(b)]. Five thermal profiles, each 10 s in duration, were recorded for each wavelength examined. Delivery of the laser radiation was controlled using a mechanical shutter (SH1; Thorlabs, Newton, New Jersey) that was triggered shortly after the start of the thermal imaging. A 2 s laser exposure was used for all wavelengths. The 1064 nm exposure was collected first, followed by stepping the OPO from 700 to 950 nm.

To generate a single measurement of the temperature rise from the spatial and temporal resolved distributions recorded by the thermal camera, a 30-pixel diameter region of interest (ROI) was assigned to the center of the laser spot. Sample

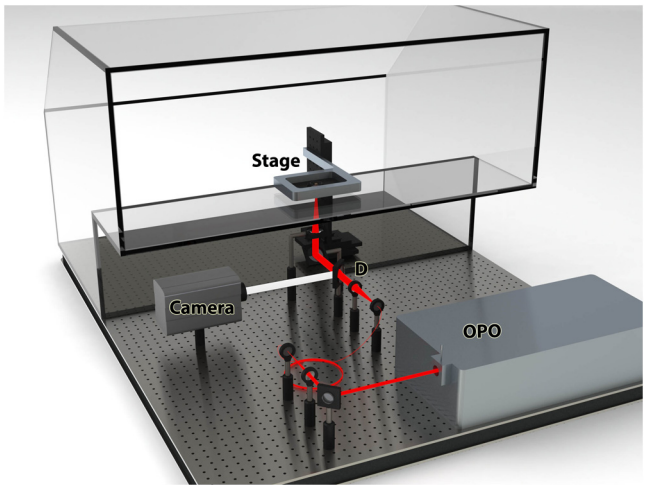

Fig. 1 Experimental setup used to measure the thermal response of tissue to laser exposure. OPO, optical parametric oscillator; D, dichroic; and Camera, FLIR thermal camera. The red beam corresponds to the excitation path and the white beam corresponds to the collected thermal signal (3 to 5 μm).

images of the thermal profile are shown for 800 and 1064 nm in Figs. 2(c)–2(r). The average temperature of the ROI prior to laser exposure was calculated and then the maximum temperature rise was found. These results, shown in Fig. 2(a), illustrate that the amount of heating drops by more than an order of magnitude as the wavelength moves deeper into the IR. This is primarily due to the decreased absorption of melanin at longer wavelengths, but is aided by lower scattering which decreases the efficiency of linear processes such as absorption.[12]

The results obtained experimentally were compared to simulated thermal profiles using a heat transfer model.[13] The BTEC thermal model, whose name is derived from its four primary authors: Buffington, Thomas, Edwards, and Clark, can be used to simulate optical radiation and radio frequency thermal interactions with tissue, and provides simulations of the temperature response of tissue and analysis of damage resulting for the thermal response. A number of damage integral values or temperature shift searches are available in order to estimate damage thresholds, or for comparison to experimental data. BTEC supports multilayered tissue models, where each layer can have different thermal, optical, and physical properties. For a more detailed description of the model and a table of the optical properties used for these simulations, see Refs. 8 and 14. Tissue perfusion was not incorporated in these simulations. Thermal profile was simulated for each wavelength examined experimentally. A 2-s exposure time and 500-μm spot were used for all wavelength simulations.

The simulated temperature rise calculated for the surface of the epidermis is depicted in Fig. 2(a). These simulated values matched well with the experimental data at all points excluding the 700- and 950-nm excitation. It is possible that tissue dehydration resulted in the lower temperature rise seen experimentally at 950 nm, as this data point was collected last after several hours of imaging. Additionally, no fitting parameters were used to account for the differences in the optical properties of the simulated tissue, such as melanin concentration, compared to the sample used. As discussed in Ref. 14, melanin determines absorption in the epidermis in the visible wavelengths, and decreases with an increasing wavelength over the range presented here. Since the tissue properties used in the simulations were derived from those reported by Salomatina, higher melanin concentrations present in the tissue studied here could result in an increase in tissue heating, especially for the shorter wavelengths.

The thermally induced damage resulting from laser-irradiated skin exposure depends on the time-temperature response of the tissue. Damage of this nature begins with local absorption of the laser energy, resulting in tissue heating. Damage can occur from this heating through denaturation of proteins, leading to subsequent apoptosis or overt necrosis. Additionally, at higher temperatures, thermal coagulation, collagen hyalinization, and changes in optical properties may be observed.[8] The damage thresholds for 700 to 1064 nm laser radiation were simulated using the BTEC model. Damage thresholds were calculated by searching for a laser power that produced a prescribed value damage integral at a 200-μm depth in the tissue using the Arrhenius damage model.[15] Tissue was assumed to

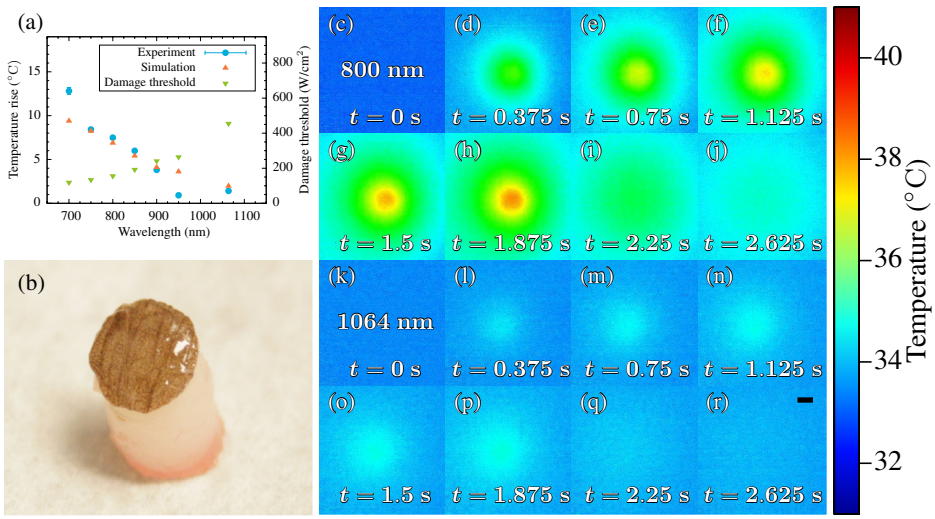

Fig. 2 (a) Temperature rise measured as a function of excitation wavelength. Simulated temperature rise and estimated damage thresholds are also displayed. (b) Tissue sample used for laser-induced heating measurements. (c)–(j) Subset of thermal images for 800-nm excitation. (k)–(r) Subset of thermal images for 1064-nm excitation. A 200-μm scale bar is included in (r).

be at body temperature (36°C) prior to laser exposure. These values are plotted in Fig. 2(a) along with the observed temperature changes. Simulated damage thresholds ranged from 119.8 to 454.8 W/cm^2 at 700 and 1064 nm, respectively.

In summary, we have presented the thermal response of bulk tissue as a function of wavelength for a fixed excitation power. Further studies are needed to examine the thermal response of tissue for wavelengths above 1064 nm as well as the impact of melanin absorption and spot size. The experiments reported here simply image the tip of an optical fiber in a tissue sample, whereas a multiphoton imaging system traditionally uses an objective lens to achieve high resolution imaging. Tissue damage as a result of the tight focal spot found in such systems needs to be considered as well as the selection of safe powers for multiphoton imaging. These experiments would have the potential to help determine the optimal excitation wavelengths for multiphoton imaging techniques to allow imaging at greater depths within tissue.

Acknowledgments

The authors acknowledge the generous support of NSF Grants (ECCS-1250360, DBI-1250361, and CBET-1250363) and the Air Force Research Laboratory, Human Effectiveness Directorate. Research performed by TASC, Inc. was conducted under USAF Contract No. FA8650-08-D-6930.

References

1. F. Helmchen and W. Denk, "Deep tissue two-photon microscopy," *Nat. Methods* **2**(12), 932–940 (2005).
2. S. W. Hell et al., "Three-photon excitation in fluorescence microscopy," *J. Biomed. Opt.* **1**(1), 71–74 (1996).
3. N. G. Horton et al., "In vivo three-photon microscopy of subcortical structures within an intact mouse brain," *Nat. Photonics* **7**(3), 205–209 (2013).
4. K. Welsher, S. P. Sherlock, and H. Dai, "Deep-tissue anatomical imaging of mice using carbon nanotube fluorophores in the second near-infrared window," *Proc. Natl. Acad. Sci. U. S. A.* **108**(22), 8943–8948 (2011).
5. L. A. Sordillo et al., "Deep optical imaging of tissue using the second and third near-infrared spectral windows," *J. Biomed. Opt.* **19**(5), 056004 (2014).
6. A. J. Welch, "The thermal response of laser irradiated tissue," *IEEE J. Quantum Electron.* **20**(12), 1471–1481 (1984).
7. B. R. Masters et al., "Mitigating thermal mechanical damage potential during two-photon dermal imaging," *J. Biomed. Opt.* **9**(6), 1265–1270 (2004).
8. J. W. Oliver et al., "Infrared skin damage thresholds from 1319-nm continuous-wave laser exposures," *J. Biomed. Opt.* **18**(12), 125002 (2013).
9. R. Arora et al., "Detecting anthrax in the mail by coherent Raman microspectroscopy," *Proc. Natl. Acad. Sci. U. S. A.* **109**(4), 1151–1153 (2012).
10. V. V. Yakovlev et al., "Stimulated Raman photoacoustic imaging," *Proc. Natl. Acad. Sci. U. S. A.* **107**(47), 20335–20339 (2010).
11. R. Arora et al., "Chemical analysis of molecular species through turbid medium," *Anal. Chem.* **86**(3), 1445–1451 (2013).
12. B. H. Hokr and V. V. Yakovlev, "Raman signal enhancement via elastic light scattering," *Opt. Express* **21**(10), 11757–11762 (2013).
13. L. J. Irvin et al., "BTEC thermal model," Technical Report # AFRL-RH-BR-TR-2008-0006, Air Force Research Laboratory, Brooks City-Base, Texas (2008).
14. E. Salomatina et al., "Optical properties of normal and cancerous human skin in the visible and near-infrared spectral range," *J. Biomed. Opt.* **11**(6), 064026 (2006).
15. A. Welch and M. van Gemert, *Optical-Thermal Response of Laser-Irradiated Tissue*, Plenum, New York (1995).